

## **Electronic Supplementary Information (ESI)**

### **Surface-mediated spin dynamics probed by optical-pump-probe scanning tunneling microscopy**

Zi-han Wang,<sup>a</sup> Cheul-hyun Yoon,<sup>a</sup> Shoji Yoshida,<sup>a</sup> Yusuke Arashida,<sup>a</sup> Osamu Takeuchi,<sup>a</sup> Yuzo Ohno<sup>a</sup> and Hidemi Shigekawa<sup>a\*</sup>

<sup>a</sup> Faculty of Pure and Applied Sciences, University of Tsukuba, Tsukuba, Ibaraki 305-8573,  
Japan

\* Corresponding address: [Hidemi@ims.tsukuba.ac.jp](mailto:Hidemi@ims.tsukuba.ac.jp)

## **STM tip and sample preparations**

An electrochemically etched tungsten tip was used for the STM and OPP-STM measurements. A GaAs (001) wafer was cleaved ( $\sim 7.5 \times 10^{-7}$  Pa) in a load-lock cell to expose a clean (110) surface. STM topography measurements including a cleavage quality check were carried out in the main chamber of the STM system ( $\sim 1 \times 10^{-8}$  Pa). Then, Mn was deposited in a preparation chamber ( $\sim 4 \times 10^{-8}$  Pa) by evaporation. Deposition procedures were conducted with identical evaporation parameters (voltage, flux, etc.), except for the deposition time, which was controlled using a mechanical shutter. After each evaporation, the sample was immediately transferred to the main STM chamber for measurement. Two types of GaAs wafer were used. Sample A was n-type Si-doped GaAs (001) with a doping concentration of  $\sim 1 \times 10^{18}$  cm<sup>-3</sup>, which was used to confirm the density of Mn deposited for different times via the STM topography, because a higher doping concentration makes STM imaging easier. Sample B was n-type Si-doped GaAs (001) with a doping concentration of  $(3.5\text{-}6.8) \times 10^{16}$  cm<sup>-3</sup>, on which OPP-STM and OPPR experiments were performed. A lower doping concentration causes larger tip-induced band bending (TIBB), increasing the intensity of the OPP-STM signal. All experiments were conducted at RT (300 K) using a VT-STM system (Scienta Omicron, Inc.)

## **OPP-STM and OPPR measurement system**

As presented in Fig.1 in the main text, two tunable femtosecond oscillators (Chameleon Ultra and Mira-HP, Coherent, Inc, 80 MHz) were synchronized (Synchrolock-AP, Coherent, Inc) in a typical master-slave configuration. OPP-STM and OPPR measurements were carried out using the same setup. Each laser can deliver  $\sim 150$  fs pulses with an average power of 3.5 W. Two ultrafast Pockels cells (Leysop Ltd., RTP-3-20 crystal) combined with  $\lambda/4$  wave plates were used to modulate the polarization states of the optical pulse trains. Pump and probe pulses were colinearly guided into the STM chamber, the diameter of the laser spot on the sample surface was estimated to be  $\sim 50$   $\mu\text{m}$ , and the laser spot position was precisely adjusted using a mirror on a piezo-driven mirror mount placed before a viewport of the chamber. For all OPP-STM measurements, a positive sample bias voltage in the range of 0.8 to 1.3 V was applied with the tunneling current set at values from 6.5 to 125 nA. The laser wavelength was set at 814 nm (1.52 eV) with an average power of  $\sim 100$  mW, measured outside the STM chamber. In the OPPR experiment, the optical conditions were adjusted

to be identical to those for OPP-STM. Instead of using the STM tip to collect the time-resolved tunneling current, a photodetector was placed outside the STM chamber to measure a reflected light.

### **Working principle of OPP-STM for probing electron spin dynamics**

To realize the observation of local time-resolved spin dynamics, we must add a measurement scheme to detect the very weak spin-related tunnel current to OPP-STM. Electron spin dynamics has been intensively studied, particularly in the ultrafast time domain by using optical methods such as time-resolved optical Kerr (Faraday) rotation spectroscopy<sup>1,2</sup>. For instance, by making use of the magneto-optical Kerr (Faraday) effect, in a typical pump-probe scheme, specific electron spins are excited using a circularly polarized pump pulse, which is followed by a time-delayed, linearly polarized probe pulse to measure the spin dynamics by measuring the rotation of the probe pulse from its initial direction under linear polarization. However, these magneto-optic-effect-based techniques cannot easily be implemented in an OPP-STM scheme. That is, to achieve fully operational OPP-STM to probe electron spin dynamics, a new electron spin excitation and detection approach is necessary.

From this perspective, the OPP-STM system presented here has a uniquely designed “polarization modulation” technique, in which laser polarization states are carefully modulated for OPP-STM to carry out nanoscale spin dynamics measurement. The system layout is schematically shown in Fig. 1 in the main text. Two ultrafast Pockels cells are precisely controlled by a laboratory-built, complex programmable logic device (CPLD)-based logic circuit to drive both of them in a well-defined timing sequence. To be more specific, using the two Pockels cells and  $\lambda/4$  waveplates, laser pulses can be modulated between two distinct polarization states: right-handed circularly polarized (R-light) and left-handed circularly polarized (L-light) states, respectively.

This laser polarization modulation technique is crucial in functionalizing OPP-STM, which is in contrast to conventional optical pump-probe spectroscopy, in which the laser intensity is commonly modulated using optical choppers. In the OPP-STM scheme, the modulation of the laser intensity will severely distort the STM tunneling current owing to the thermal effect applied to the tip<sup>3,4</sup>. Therefore, for the spin detection, there is no active modulation of the laser intensity. Additionally, although the intensity of the R-light is produced equally to that of the

L-light in this high-speed polarization modulation technique, polarization can be unintentionally modulated owing to the polarization dependence of the reflectance on the optics. This passive laser intensity modulation must also be minimized. We have introduced a new modulation technique to overcome the above problems.

It is necessary to highlight that, for the two Pockels cells, a slight frequency difference is intentionally introduced, for example, polarization modulation is carried out on one Pockels cell at 1 MHz and on the other Pockels cell at 0.999 MHz, as shown in Fig. 1 in the main text. Here, this difference in the modulation frequency of  $\Delta f = 1 \text{ MHz} - 0.999 \text{ MHz} = 1 \text{ kHz}$  is essential for obtaining a time-resolved, spin-related tunneling current in this OPP-STM scheme. Specifically speaking, by providing a modulation frequency difference  $\Delta f$ , consecutive phase shifts in the relative circularly polarization states will occur between pump and probe pulses. Consequently, this modulation frequency difference  $\Delta f$  gives rise to two distinct polarization modes: one polarization mode is named “co circular polarization (co-CP)”, in which pump and probe pulses have identical polarization states; the other polarization mode is named “counter-circular polarization (counter-CP)”, in which pump and probe pulses always have opposite polarization states. These two polarization modes switch back and forth at  $\Delta f = 1 \text{ kHz}$ . In fact, these modes contribute differently to the photocarrier density  $n_{\text{ex}}$  as a function of delay time, and the differential photo-carrier density  $\Delta n_{\text{ex}}$  can be reflected in the STM tunneling current via polarization modulation. If we define the co- (counter-) CP-determined tunneling current as  $I^{\text{co}}(t_d)$  ( $I^{\text{counter}}(t_d)$ ), as the STM tunneling current  $I$  is proportional to  $n_{\text{ex}}$ , the relaxation of electron spin can be reflected in the lock-in detected differential tunneling current, which can be qualitatively represented as  $\Delta I(t_d) = I^{\text{counter}}(t_d) - I^{\text{co}}(t_d)$ . See ref. 5 for more details.

### Fitting procedures and definition of lifetime

For both OPP-STM and OPPR results (Figs. 3 and 4 in the main text), fitting was carried out using the following single exponential function:

$$f(t) = A \exp\left\{-\frac{(t-t_0)}{\tau}\right\} + B \quad (1)$$

where  $A$  = amplitude;  $t_0$  = zero-delay position;  $\tau$  = decay constant;  $B$  = background (baseline).

In the experiment,  $t_0$  was well calibrated using the autocorrelation method by adjusting the optical delay time  $t_d$  between the pump and probe pulses to have the value at which the strongest optical interference occurred.

It is also important to state that our OPP-STM (and OPPR) method is a spin-dependent, differential-absorption-based method, as previously explained. In other words, this approach itself probes the overall mixture of “up-spin” and “down-spin” electron, with consideration of the rate equations

$$\begin{aligned}\frac{dN_{\uparrow}}{dt} &= -\frac{N_{\uparrow}}{\tau_r} - \frac{N_{\uparrow}}{\tau_s} + \frac{N_{\downarrow}}{\tau_s} \\ \frac{dN_{\downarrow}}{dt} &= -\frac{N_{\downarrow}}{\tau_r} - \frac{N_{\uparrow}}{\tau_s} + \frac{N_{\downarrow}}{\tau_s}\end{aligned}\quad (2)$$

Here,  $N_{\uparrow}$  is the density of electrons with an “up-spin” orientation, whereas  $N_{\downarrow}$  is the density of electrons with a “down-spin” orientation, respectively.  $\tau_r$  is the carrier recombination lifetime and  $\tau_s$  is the spin relaxation time, or spin lifetime. By solving Eq. (2), we obtain

$$\begin{aligned}N_{\uparrow} &= \frac{N_0}{2} \left\{ 1 + \exp\left(\frac{-2t}{\tau_s}\right) \right\} \exp\left(\frac{-t}{\tau_r}\right) \\ N_{\downarrow} &= \frac{N_0}{2} \left\{ 1 - \exp\left(\frac{-2t}{\tau_s}\right) \right\} \exp\left(\frac{-t}{\tau_r}\right)\end{aligned}\quad (3)$$

Here,  $N_0$  is defined as the initial value of  $N_{\uparrow}$ . From Eq. (3), it is clear that

$$N_{\uparrow} - N_{\downarrow} = N_0 \exp\left(\frac{-2t}{\tau_s}\right) \exp\left(\frac{-t}{\tau_r}\right) \quad (4)$$

Note that in the n-type GaAs sample we used for experiments, at room temperature (300 K) the carrier lifetime ( $\tau_r \sim 5$  ns<sup>9</sup>) is significantly longer than the spin lifetime ( $\tau_s < 500$  ps). Therefore,  $\tau$  in Eq. (1) can be expressed as  $\tau = \tau_s/2$ .

### Penetration depth determination

A simple calculation was carried out as follows to obtain the penetration depth in our case.

The optical penetration depth of  $\sim 800$  nm light in GaAs with normal incidence geometry is  $\sim 1 \mu\text{m}$ <sup>10,11</sup>. The incident angle in our experimental configuration is shown in Fig. S4(a) and a

schematic illustration is shown in Fig. S4(b). On the basis of well-known Snell's Law, with an incident angle of  $31^\circ$ , the refracted light angle with respect to the sample normal becomes  $13.5^\circ$ , where refraction indexes of the vacuum and GaAs of  $n_{\text{vac}} = 1$  and  $n_{\text{GaAs}} = 3.67$  were used, respectively. In general, the optical penetration depth  $\delta$ , which is the depth at which the laser intensity of the transmitted (refracted) light drops to  $1/e$  of its initial value at the incidence interface, is defined as<sup>12</sup>

$$\delta = \frac{1}{\alpha} \quad (5)$$

Here,  $\alpha$  is the absorption coefficient of the material at a certain wavelength and temperature. In the case of our GaAs sample excited by 814 nm pulses at 300 K,  $\alpha \sim 12764 \text{ cm}^{-1}$  (see Ref. 13). Thus, by using Eq. (5) under an oblique incidence geometry (refracted angle of  $13.5^\circ$ ), we

estimated the penetration depth to be  $\delta^* = \frac{1}{\alpha} \frac{1}{\cos(13.5^\circ)} \sim 800 \text{ nm}$ .

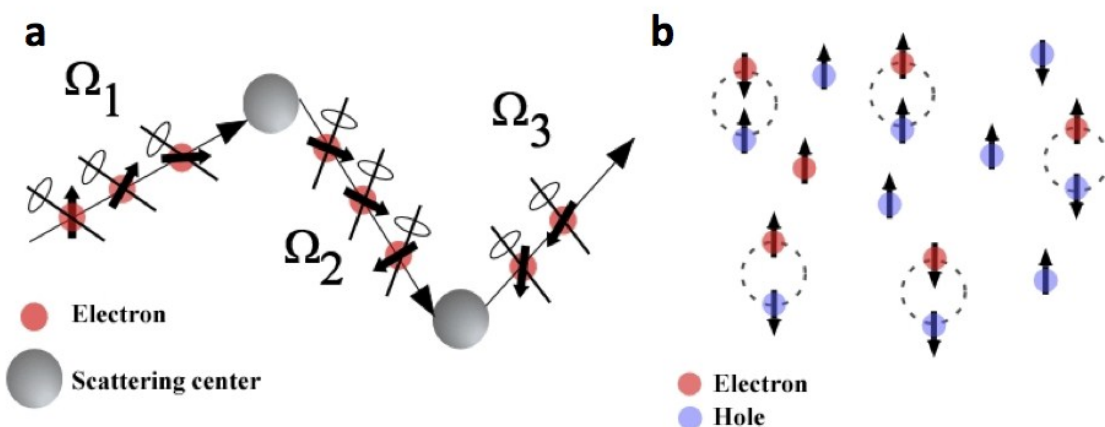


**Fig. S1** Two spin relaxation mechanisms involved in the system under investigation. (a) Dyakonov-Perel (DP) spin relaxation mechanism<sup>6</sup>. Small red balls represent electrons, whereas larger gray balls represent scattering centers.  $\Omega_n$  ( $n = 1, 2, 3$ ) are microscopic magnetic fields with different magnitudes and directions, which force electrons to precess around each magnetic field axis between the two subsequent scattering events, leading to spin relaxation. (b) Bir-Aronov-Pikus (BAP) spin relaxation mechanism<sup>6</sup>. Red and blue balls represent electrons and holes, respectively. In this case, electron spins relax owing to the electron-hole spin exchange interaction. The effect of potential modulation by Mn acceptor ( $2 \times 10^{18} \text{ cm}^{-3}$ ) in a dark condition works in the range of 10 nm<sup>7</sup>. When surface Mn density is further increased, it may be necessary to consider the effect that the potential becomes smoother in addition to the BAP effect. Details including the screening effect under photo illumination. Details while photo excitation process are left for future work.

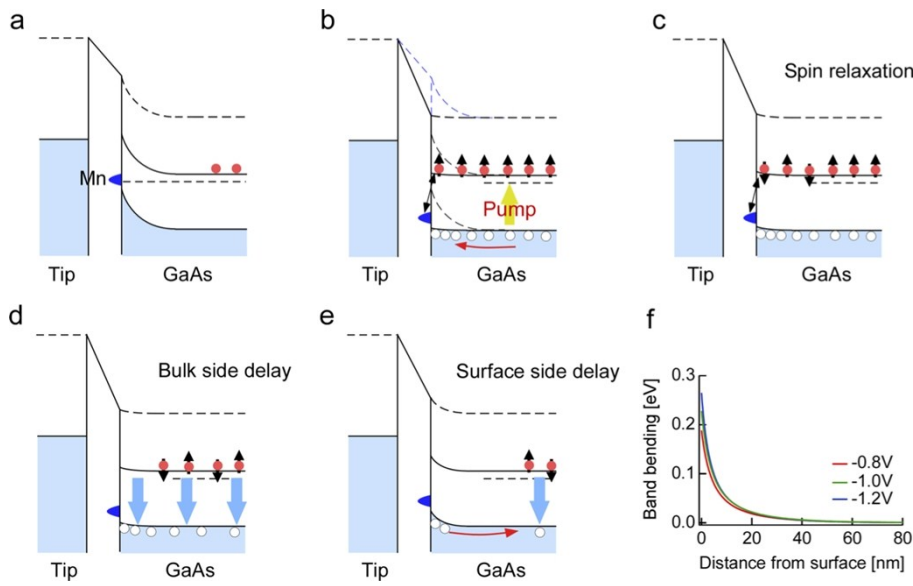


**Fig. S2** A model for producing spin-related OPP-STM signal and results of simulations of TIBB. (a) TIBB under dark condition. (b) Excitation by pump pulse. The electric field and thus the surface potential are reduced, increasing the effective bias voltage applied to the tunnel junction (surface photovoltage: SPV). Consequently, the photoexcitation increases the transient tunnel current. For simplicity spin orientation was presented as 100 %. (c) to (e), The excited state subsequently relaxes to the original state via three processes: the randomization of spin orientation (c), the decay of photocarriers via recombination (d), diffusion and drift, and the decay of minority carriers transiently trapped at the surface during the photoexcitation via thermal emission or recombination at the Mn site with the tunnel current from the STM tip (e)<sup>8</sup>. When a probe pulse arrives during the relaxation processes, an additional SPV is induced, which changes the total magnitude of the tunnel current depending on the delay time,  $t_d$ , providing time-resolved spectra. (f) Simulated TIBB. Calculations were carried out using SEMTiP Fortran Package provided by Feenstra (CMU) for the three typical applied bias voltages used in this experiment. For a GaAs sample we used the doping level of  $3.8\text{--}6.2 \times 10^{16}$  cm<sup>-3</sup>, and the TIBB depth is ~40 nm even in a dark condition and becomes close to flat under photo illumination, which is much shorter than the optical penetration depth of ~800 nm. Detailed analysis while excitation and relaxation are left for a future work.

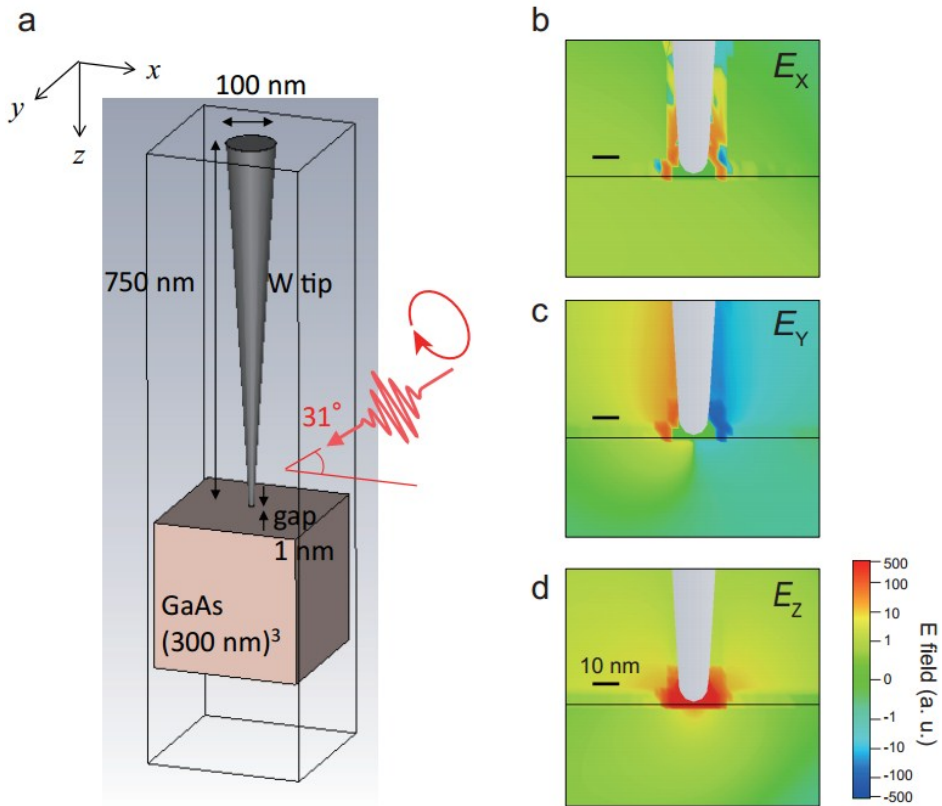


**Fig. S3** Results of simulations for the electric fields modulated by the STM tip. (a) Schematic illustration of the experimental setup used for the simulation. (b)-(d), Maps of the strength of the electric fields of the  $x$ -,  $y$ - and  $z$ -components of circularly polarized light. Time-domain calculations of electromagnetic wave propagation were carried out using CST Studio Suite. A tungsten (W) tip and a GaAs sample were arranged at a distance of 1 nm. The W tip was a truncated cone and its apex was spherical shape with a diameter of 10 nm. Circularly polarized light with a center frequency of 370 THz ( $\lambda = 814$  nm) was used as the incident electromagnetic wave with an angle of 31° from the horizontal plane. The minimum mesh of the space was 2.5 nm. The black line in the maps indicate the position of the sample surface. In the case of a W tip, the tip-induced electric-field enhancement in the  $z$ -direction is about 400 times the incident light intensity around the tip apex, which sharply decreases inside the sample with increasing distance from the surface. Therefore, the excitation by the circularly polarized light condition below the STM tip is initially disturbed around the tip apex but then recovers at a depth of a few nm.

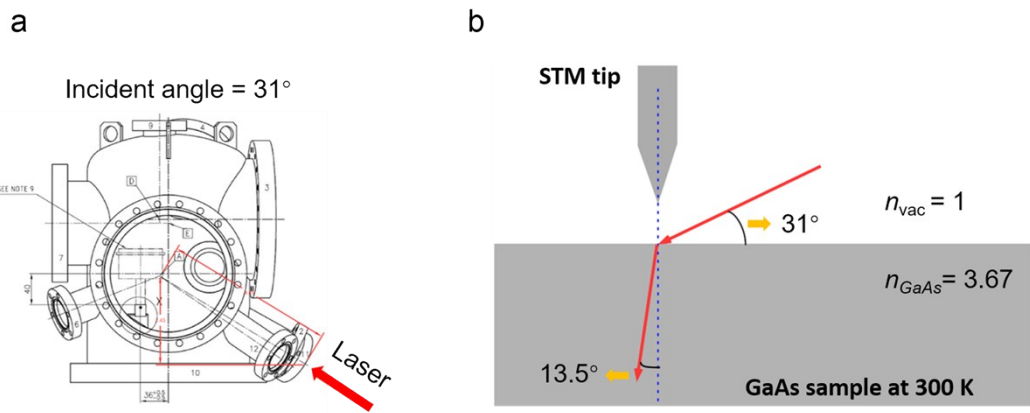


**Fig S4.** (a) Experimental setup. Both OPP-STM and OPPR measurements were conducted using an STM UHV chamber, at a fixed laser incident angle of  $\sim 31^\circ$ . (b) Schematic illustration of the geometry of the oblique incidence light and the refracted light that penetrates into the sample, which determines the optical penetration depth.

**Reference:**

1. A.V. Kimel, F. Bentivegna, V. N. Gridnev, V. V. Pavlov, R. V. Pisarev and Th. Rasing, *Phys. Rev. B.*, 2001, **63**, 235201.
2. J. A. Gupta, D. D. Awschalom, X. Peng and A. P. Alivisatos, *Phys. Rev. B.*, 1999, **59**, R10421.
3. R. Huber, M. Koch and J. Feldmann, *Appl. Phys. Lett.*, 1998, **73**, 2521.
4. H. Shigekawa, S. Yoshida, O. Takeuchi, M. Aoyama, Y. Terada, H. Kondo and H. Oigawa, *Thin solid films*, 2008, **516**, 2384.
5. S. Yoshida, Y. Aizawa, Z. H. Wang, R. Oshima, Y. Mera, E. Matsuyama, H. Oigawa, O. Takeuchi and H. Shigekawa, *Nat. Nanotechnol.*, 2014, **9**, 588.
6. M. I. Dyakonov, Spin Dynamics in Semiconductors: *Springer Series in Solid-State Sciences* **157**, Springer, 2008.
7. S. Yoshida, Y. Kanitani, O. Takeuchi and H. Shigekawa, *Appl. Phys. Lett.*, 2008, **92**, 102.
8. M. Yokota, S. Yoshida, Y. Mera, O. Takeuchi, H. Oigawa and H. Shigekawa, *Nanoscale*, 2013, **5**, 9170.
9. Y. Terada, S. Yoshida, O. Takeuchi and H. Shigekawa, *Nat. Photon.*, 2010, **12**, 869.
10. M. Schall and P. U. Jepsen, *Opt. Lett.* 2000, **25**, 13.
11. M. C. Beard, G. M. Turner, and C. A. Schmuttenmaer, *Phys. Rev. B.*, 2000, **62**, 15764.
12. M. S. Brown and C. B. Arnold, *Laser Precision Microfabrication: Springer Series in Materials Science*, **135**, Chapter 4, 2010.
13. D. E. Aspnes, S. M. Kelso, R. A. Logan and R. Bhat, *J. Appl. Phys.*, 1986, **60**, 754.